Applied Physics B (2022) 128:220
https://doi.org/10.1007/s00340-022-07938-0

Applied Physics B
Lasers and Optics

RESEARCH

Transportable 30 cm optical cavity based ultrastable lasers with beating instability of 2×10^{-16}

Rui Xiao[1,2] · Yanqi Xu[1] · Yan Wang[1] · Huanyao Sun[1] · Qunfeng Chen[1]

Received: 11 August 2022 / Accepted: 9 November 2022 / Published online: 28 November 2022

Abstract
Transportable ultrastable lasers (TUL) are the key parts of transportable optical clocks. In the previous works, TUL were based on transportable optical cavities with lengths of about 10 cm, which limited the stability of the TUL to middle term of 10^{-16}. In this work, we designed two transportable cavities with lengths of 30 cm and built two TULs with frequency stabilities close to the thermal noise limit of the cavities. The cavities are mounted by squeezing with slim posts on symmetric planes. The mounting method guarantees that the cavities are robust, transportable, and at low vibration sensitivities of $< 5 \times 10^{-10}/\mathrm{g}$. The most probable linewidth of the beating between the two lasers is 0.14 Hz. The minimal instability of the beating frequency is 2.0×10^{-16}, which happens at 0.5 s averaging time, and increases slowly to 3.2×10^{-16} at the averaging time of 100 s. This result is more than 2 times better than previous reported TUL. The design of the cavities may promote the research of transportable optical clock to the level of small coefficient of 10^{-18}.

1 Introduction

Ultrastable lasers are the essentials for precision spectroscopy and fundamental physics measurements, e.g. optical clocks [1–3], gravitational wave detection [4, 5], local Lorentz invariance demonstration [6–8]. An ultrastable laser is built by locking of the laser frequency to the resonance of a ultrastable Fabry-Pérot cavity. The stability of the ultrastable laser is fundamentally limited by the thermal noises of the cavity [9–11]. Changing the material of cavity mirror's substrates to fused silica (FS) glass, extending the length of the cavity, and replacing the coating layers of the mirrors to crystalline coating [12] are the ways to reduce the thermal noise of the room temperature cavities. Currently, the long room temperature reference cavities for using in the laboratory are with lengths of about 30 cm to 50 cm and the corresponding instabilities of the lasers are 1.5×10^{-16} to 0.8×10^{-16} [13–16].

For systems used outside of laboratory, e.g. transportable optical clocks [17–19], space optical clocks [20], space gravitational wave detection [21–23], ultrastable lasers are required to be transportable [24]. Therefore, the reference cavities have to be fixed robustly and keep vibration insensitive. There are several typical designs of transportable cavities [25–28]. Because these transportable cavities were with the lengths of about 10 cm, the thermal noise of the cavity limited the modified frequency stability to a level of $> 3 \times 10^{-16}$ [28]. To obtain transportable ultrastable laser with lower frequency instability, longer transportable cavities are required.

In this work, we present two ultrastable lasers based on 30 cm transportable cavities with frequency instabilities close to the cavities' thermal noise limit and reach the level of 1.4×10^{-16}. The cavities are mounted by squeezing on the symmetric planes in the three orthogonal directions with slim posts, which guarantee the cavities are transportable and insensitive to vibration. Two stages of temperature

✉ Qunfeng Chen
qfchen@apm.ac.cn

Rui Xiao
xiaorui@apm.ac.cn

Yanqi Xu
xuyanqi@apm.ac.cn

Yan Wang
wangy@apm.ac.cn

Huanyao Sun
sunhuanyao@apm.ac.cn

[1] State Key Laboratory of Magnetic Resonance and Atomic and Molecular Physics, Innovation Academy for Precision Measurement Science and Technology, Chinese Academy of Sciences, Wuhan 430071, China

[2] University of Chinese Academy of Sciences, Beijing 100049, China

stabilization are applied to the cavity system. One is on the vacuum chamber and the other is inside it. The outer stage supplies a stable temperature environment, while the inner stage controls the temperature to the zero thermal expansion temperature (ZTET) of the cavity. Brewster cut electro-optic modulators (EOM) are used to supply a low residual amplitude modulation (RAM) phase modulation for Pound-Drever-Hall (PDH) frequency locking. The minimal Allan deviation of beat frequency between them is about 2×10^{-16} at the averaging time of 0.5 s. The most probable linewidth of the beat signal is 0.14 Hz.

2 Design and properties of the cavity system

The design and supporting method of the two cavities are the same. The design of the cavity is shown in Fig. 1. The cavity spacer is cut from a piece of standard grade ultra-low expansion (ULE) glass cuboid with size of $300 \times 100 \times 100$ cm^3. The cavity mirrors are made of FS glass to reduce the thermal noise. ULE rings are attached to the outer side of the mirror to compensate the thermal expansion of the mirrors [29].

The cavities are highly reflective coated for 1064 nm. The linewidths of the cavities were measured to be 1.6 kHz and 2.3 kHz, and the corresponding finesse were 310,000 and 220,000, respectively. The fractions of laser power coupled into the cavity were 48 % and 35 %.

The supporting method follows the previous design on the 10 cm transportable cavities [27, 30]. Three sets of slim posts are used to mount the cavity by squeezing from 3 orthogonal directions. The cross-cavity supports are cut out of the spacer, and the along-cavity supports are Invar stubs glued on the spacer. Fluororubber balls are used as the buffer between the posts and the spacer. Each set of posts limit the movement of the cavity from one direction. The three sets of posts limit the movement of the cavity from all directions.

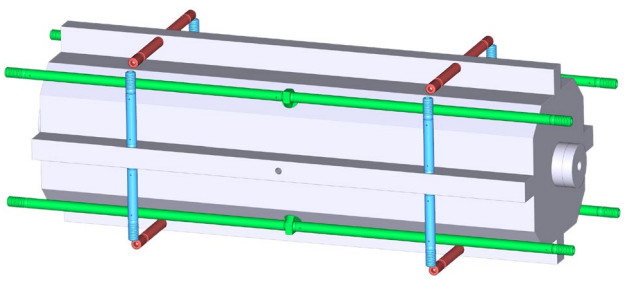

Fig. 1 Design and the supporting method of the cavity. The gray color indicates the cavity. The green, blue, and red color sticks indicate the supporting posts

The shape and support of the cavity are symmetric according the supporting center planes. The symmetric design guarantees that the distance between the cavity mirror centers (DCMC) is insensitive to acceleration in all directions. The mirror will tilt under the accelerations crossing the cavity, which is minimized using finite element analyze (FEA). A quarter of the cavity is used to perform the optimization. The simulation results are shown in Fig. 2. Fig. 2a shows the along-cavity deformation under a 1 g's crossing cavity acceleration in pseudo color. It shows that the along-cavity displacement of the cavity mirror is less than 2×10^{-11} m under the acceleration. Fig. 2b shows that the sensitivity of the DCMC is fluctuated at a level $\pm 5 \times 10^{-12}/g$ around 0, which was limited by the FEA model. Fig. 2c shows that the slope of tilt sensitivity of the cavity mirror versus the supporting position is about 6 nrad$\cdot g^{-1}$/mm and the minimum tilt happens at around 90.5 mm from the center of the cavity.

The beat frequency and the corresponding acceleration variation with time are present in Fig. 3. From the figure, the vibration sensitivities of the two cavities were calculated to be 2.4×10^{-10}/g, 2.6×10^{-10}/g, 4.4×10^{-10}/g; 3.1×10^{-10}/g, 2.7×10^{-10}/g, and 4.0×10^{-10}/g for the vertical, horizontal, and axial directions of the two cavities, which were similar to that of stationary cavities.

The section view of the cavity mounted in the vacuum chamber is shown in Fig. 4. The green color indicates the supporting frame and aluminum plates covering the frame. The supporting posts are fixed to the frame by threaded holes. Squeezing force to the cavity is adjusted by controlling the depth of screws. The aluminum plates supply one layer of thermal shield for the cavity, which build a mounting box (MB) for the cavity. The MB is fixed to an active temperature stabilization box (ATSB) (orange in the figure). Two pieces of 1 mm thick Poly tetra fluoroethylene (PTFE) layer are used to isolate the thermal contact between the MB and the ATSB. The ATSB is placed on thermoelectric coolers (TEC) for controlling the temperature of the cavity. The other side of the TECs are attached to the bottom of the vacuum chamber (VC, blue in the figure). Another set of TECs is placed under the chamber for stabilizing the temperature of the VC. The size of the chamber is $480 \times 265 \times 228$ mm^3. The total weight of the cavity with the chamber is about 41 kg.

The vacuum and thermal properties of the cavities are similar. The vacuums of chambers are kept at about 2×10^{-7} Pa by using 10 L/s ion pumps. The time constants of the temperature transmission from the ATSB to the cavity are about 50 hours. Homemade temperature controllers are used to stabilize the temperatures. The stabilities at the controlling points are shown in Fig. 5. One is on the vacuum chamber for supplying a stable temperature surrounding, which is stabilized to about 22 °C. The other is on the

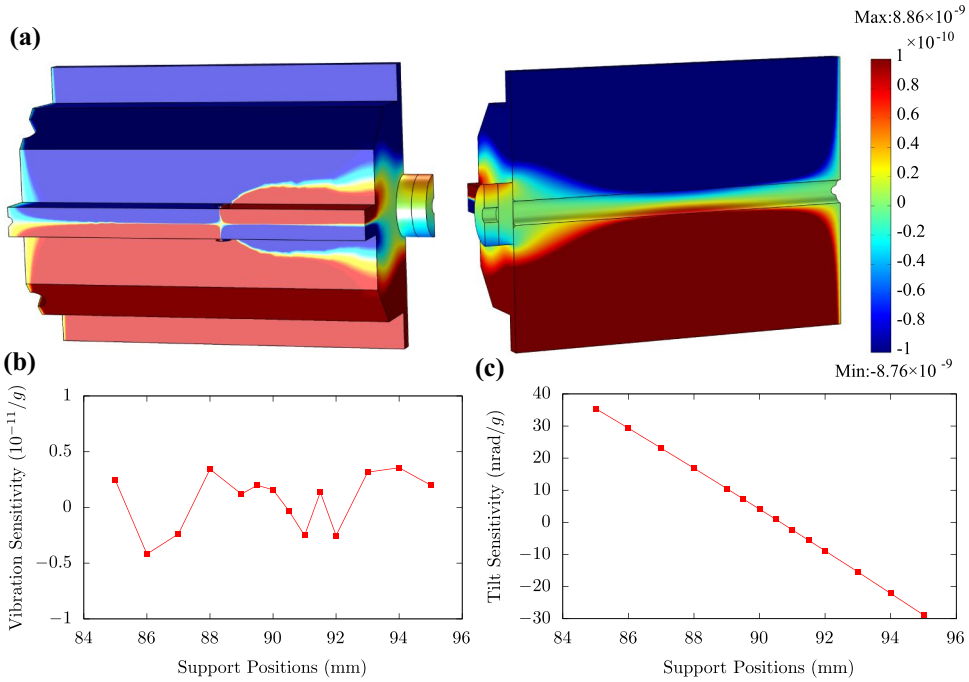

Fig. 2 FEA result on a quarter of the cavity under 1 g's cross cavity acceleration. **a** the pseudo color figures of the displacement along the cavity axis. The unit shown in the figure is meter. **b** sensitivity of the DCMC to the supporting positions. **c** tilt sensitivity of the cavity mirror to the supporting positions

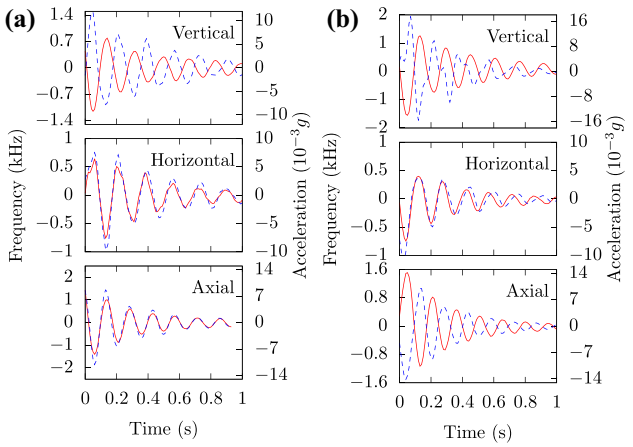

Fig. 3 Beat frequency variations (red line) and the corresponding accelerations (blue dashed line) under disturbances along difference directions. Left panel **a** is for cavity 1 and right panel **b** is for cavity 2

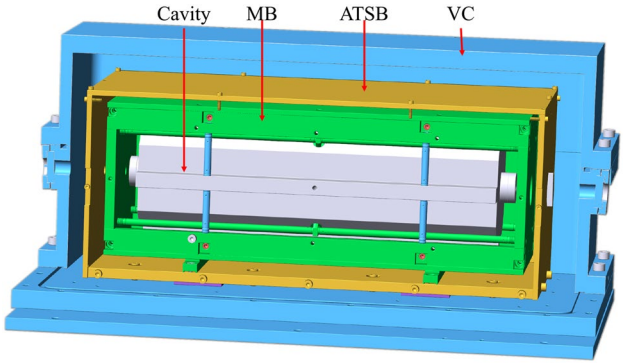

Fig. 4 Section view of the cavity mounted in the vacuum chamber. MB indicates the mounting box for the cavity. ATSB indicates the active temperature stabilizing layer. VC indicates the vacuum chamber

ATSB, which stabilizes the temperature to the ZTET of the cavity (about 5 °C) to reduce the influence of temperature fluctuation to cavity length. The stability of the temperature at the controlling point of the ATSB is better than 100 μK.

3 Design and performance of the lasers

The optical setup of the ultrastable lasers is shown in Fig. 6. It is mainly a standard PDH locking scheme [31]. Nd:YAG lasers are used as the laser sources. Efforts are made to improve stability of the lasers. To reduce RAM

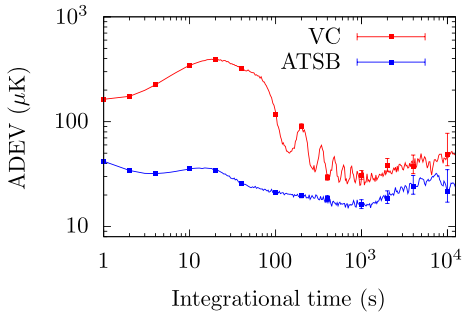

Fig. 5 Allan deviation of the temperatures at the controlling points

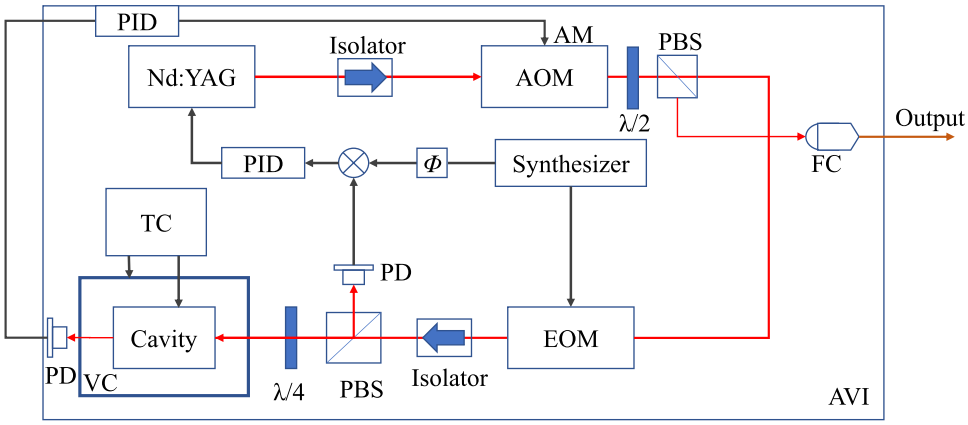

Fig. 6 Schematic of the optical setup. The abbreviations in the figure mean follows, Nd:YAG, Nd:YAG laser; Isolator, optical isolator; AOM, acousto-optical modulator; $\lambda/2$, half-wave plate; PBS, polarized beam splitter; FC, optical fiber collimator; EOM, electro-optic modulator; $\lambda/4$; quarter-wave plate; TC, temperature controller; PD, photodetector; PID, proportional-integral-derivative circuit; Φ phase shifter; AM, amplitude modulation

in the optical setup, temperature stabilized Brewster-cut parallelogram electro-optic modulators (EOM) are used to generate the PDH modulation [32, 33]. Optical isolators are inserted between the EOM and the cavity to stop the interference in the optical path. Additional photodetector (PD) is used to detect the transmission power of the cavity and feedback to stabilize the laser power in the cavity via an acousto-optical modulator (AOM) to reduce the cavity length variation caused by the heating effect of the laser power. 2-stage proportional-integral-derivative (PID) circuits are used to lock the laser frequency and power. The residual frequency instability caused by the RAM, frequency and power locking circuits are shown in Fig. 8c as the green, olive, and purple lines. The voltage level of these factors are similar. The different coefficients of voltage to frequency causes the different level on the equivalent frequency stability. The residual frequency instabilities are several times lower than the thermal noise limit of the cavity. The optical setup is laid on an active-vibration-isolation (AVI) table to isolate vibration from the floor. The frequency instability caused by the residual vibration is shown as the teal line in Fig. 8c. The vibration sensor is AC coupled and can only be measured to about 1 Hz.

The outputs of the lasers were combined using a fiber beam splitter for measuring their beat frequency and testing the performance of the lasers. The beating frequency between the two lasers was about 18 MHz, and the relative drift was about -2.5 mHz/s.

The linewidth of the beating frequency was measured using Stanford Research Systems SR785. The beat signal was downmixed with a frequency synthesizer to about 50 kHz and sent to the SR785. The -2.5 mHz/s drift was compensated using the sweep function of synthesizer. Each spectrum was captured with 32 s duration. The width of each bin in the spectrum were 0.03125 Hz. Totally 262 spectra were captured continuously. The spectra were fit with Lorentz function. The statistic of the FWHM of the spectra is shown in Fig. 7a. The bar width in Fig. 7a is 0.025 Hz. The most probable linewidth obtained using Gaussian fitting of the statistic is 0.137 ± 0.014 Hz. The spectra were center overlapped and fit with Lorentz function. The result is shown in Fig.7b. The average linewidth of the beat signal obtained from the fitting was 0.192 ± 0.001 Hz.

The beating frequency was recorded using a Keysight 53220A with gate time of 1 s for long-term measurement and Microsemi 3120A with gate time of 1 ms for short-term and phase noise measurement. A beating frequency trace of 6×10^4 s measured by 53220A with linear drift of -2.52 mHz/s removed is shown in Fig. 8a. It shows that the beat frequency fluctuated in a range of ± 4 Hz. The fluctuation was caused by the temperature fluctuation in the laboratory. The frequency noise of the beat signal calculated from the 3120A phase noise measurement and the beat trace in

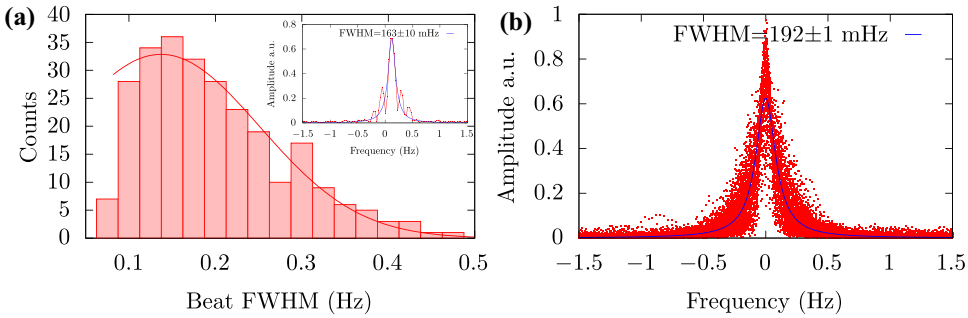

Fig. 7 Linewidth property of the beating spectra. **a** statistic of the linewidth distribution. The red line is the Gaussian fitting of the distribution. The inset shows an example of the beating spectrum with Lorentz fitting. **b** Lorentz fitting of the center overlapped spectra

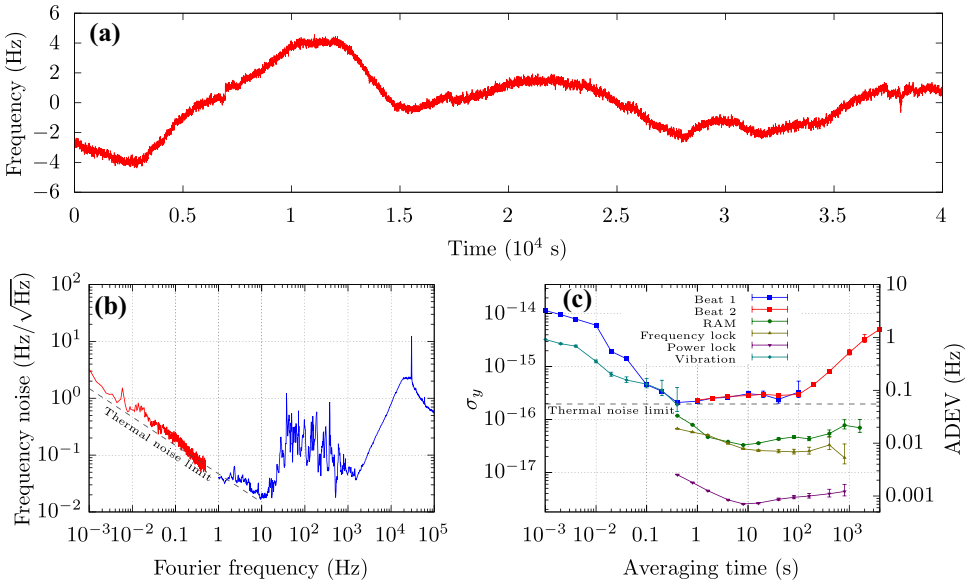

Fig. 8 Characterization of beat frequency stability. **a** beat frequency trace with linear drift of -2.52 mHz/s removed. **b** frequency noise of the beat signal. The red line was calculated from the trace shown in **a**. The blue trace was calculated from the phase noise measured by 3120A. **c** Allan deviation of the beat frequency. The red line was calculated from the trace shown in **a**. The blue line was calculated from a 10 minutes measurement using 3120A. The grey lines dashed in **b** and **c** were the estimated thermal noise limit of the beat signal which was 2×10^{-16}. The other lines were estimated equivalent residual frequency instability of the system

Fig. 8a is shown in Fig. 8b. The Allan deviations of the trace and the beating frequency measured by 3120A are shown in Fig. 8c as the red and blue traces, respectively. The figure shows that the Allan deviation of the beat frequency reaches a minimal value of 55 mHz (2×10^{-16}) at the averaging time of 0.5 s, and slowly increases to 65 mHz (2.3×10^{-16}) and 90 mHz (3.2×10^{-16}) at the averaging time of 1 s and 100 s respectively. With averaging time of longer than 50 s, the Allan deviation is limited by room temperature fluctuation. The frequency stability for each single laser is estimated to be 1.4×10^{-16}, 1.6×10^{-16} and 2.3×10^{-16} at the averaging time of 0.5 s, 1 s and 100 s, respectively, by dividing the beat frequency stability with $\sqrt{2}$.

The two systems were built in the laboratory on the third floor and then transported to the laboratory underground. The lasers worked without any downgrade after the transportation, which demonstrated the advantage of the design compared with stationary designs.

4 Conclusion

In conclusion, we report two thermal noise limited ultrastable lasers based on two transportable 30 cm cavities. The fractional frequency instability of each laser is 1.4×10^{-16} and 2.3×10^{-16} at the averaging time of 0.5 s and 100 s. The work demonstrated that the robust squeezing mounting method did not bring observable noise limit to the 30 cm room temperature cavity. The limit of the laser frequency instability may be further reduced by replacing the coating of the cavity mirrors with crystalline coating. The ultrastable lasers are currently used as the reference lasers for our optical frequency comparison and conversion station [34, 35].

Funding National Key R &D Program of China, Grant No. 2020YFA0309801 and 2017YFA0304403, the Strategic Priority Research Program of the Chinese Academy of Sciences, Grant No. XDB21010300 and XDB21030100, National Natural Science Foundation of China, Grant No. 91636110 and U1738141.

Declarations

Conflict of interest The authors declare that there are no conflicts of interest related to this article.

References

1. P. Gill, Optical frequency standards. Metrologia **42**(3), S125–S137 (2005)
2. A.D. Ludlow, M.M. Boyd, J. Ye, E. Peik, P.O. Schmidt, Optical atomic clocks. Rev. Mod. Phys. **87**(2), 637–701 (2015)
3. E. Oelker, R.B. Hutson, C.J. Kennedy, L. Sonderhouse, T. Bothwell, A. Goban, D. Kedar, C. Sanner, J.M. Robinson, G.E. Marti, D.G. Matei, T. Legero, M. Giunta, R. Holzwarth, F. Riehle, U. Sterr, J. Ye, Demonstration of 4.8×10^{-17} stability at 1 s for two independent optical clocks. Nat. Photon. **13**(10), 714 (2019)
4. B.P. Abbott, R. Abbott, R. Adhikari et al., LIGO: The laser interferometer gravitational-wave observatory. Rep. Prog. Phys. **72**(7), 076901 (2009)

5. B.P. Abbott, R. Abbott, T.D. Abbott et al., Observation of gravitational waves from a binary black hole merger. Phys. Rev. Lett. **116**(6), 061102 (2016)
6. H. Müller, P.L. Stanwix, M.E. Tobar, E. Ivanov, P. Wolf, S. Herrmann, A. Senger, E. Kovalchuk, A. Peters, Tests of relativity by complementary rotating Michelson-Morley experiments. Phys. Rev. Lett. **99**(5), 050401 (2007)
7. C. Eisele, A.Y. Nevsky, S. Schiller, Laboratory test of the isotropy of light propagation at the 10^{-17} level. Phys. Rev. Lett. **103**(9), 090401 (2009)
8. Q. Chen, E. Magoulakis, S. Schiller, High-sensitivity crossed-resonator laser apparatus for improved tests of Lorentz invariance and of space-time fluctuations. Phys. Rev. D **93**(2), 022003 (2016)
9. Y. Levin, Internal thermal noise in the LIGO test masses: a direct approach. Phys. Rev. D **57**(2), 659–663 (1998)
10. K. Numata, A. Kemery, J. Camp, Thermal-noise limit in the frequency stabilization of lasers with rigid cavities. Phys. Rev. Lett. **93**(25), 250602 (2004)
11. T. Kessler, Thomas Legero, U. Sterr, Thermal noise in optical cavities revisited. J. Opt. Soc. Am. B **29**(1), 178–184 (2012)
12. G.D. Cole, W. Zhang, M.J. Martin, J. Ye, M. Aspelmeyer, Tenfold reduction of Brownian noise in high-reflectivity optical coatings. Nat. Photon. **7**(8), 644–650 (2013)
13. Y.Y. Jiang, A.D. Ludlow, N.D. Lemke, R.W. Fox, J.A. Sherman, L.S. Ma, C.W. Oates, Making optical atomic clocks more stable with 10^{-16}-level laser. Nat. Photon. **5**(3), 158–161 (2011)
14. L. Jin, Y. Jiang, Y. Yao, H. Yu, Z. Bi, L. Ma, Laser frequency instability of 2×10^{-16} by stabilizing to 30-cm-long Fabry-Perot cavities at 578 nm. Opt. Express **26**(14), 18699–18707 (2018)
15. T.L. Nicholson, M.J. Martin, J.R. Williams, B.J. Bloom, M. Bishof, M.D. Swallows, S.L. Campbell, J. Ye, Comparison of two independent Sr optical clocks with 1×10^{-17} stability at 10^3 s. Phys. Rev. Lett. **109**(23), 230801 (2012)
16. S. Häfner, S. Falke, C. Grebing, S. Vogt, T. Legero, M. Merimaa, C. Lisdat, U. Sterr, 8×10^{-17} fractional laser frequency instability with a long room-temperature cavity. Opt. Lett. **40**(9), 2112 (2015)
17. J. Grotti, S. Koller, S. Vogt, S. Hafner, U. Sterr, C. Lisdat, H. Denker, C. Voigt, L. Timmen, A. Rolland, F.N. Baynes, H.S. Margolis, M. Zampaolo, P. Thoumany, M. Pizzocaro, B. Rauf, F. Bregolin, A. Tampellini, P. Barbieri, M. Zucco, G.A. Costanzo, C. Clivati, F. Levi, D. Calonico, Geodesy and metrology with a transportable optical clock. Nat. Phys. **14**(5), 437 (2018)
18. Y. Huang, H. Zhang, B. Zhang, Y. Hao, H. Guan, M. Zeng, Q. Chen, Y. Lin, Y. Wang, S. Cao, K. Liang, F. Fang, Z. Fang, T. Li, K. Gao, Geopotential measurement with a robust, transportable Ca^+ optical clock. Phys. Rev. A **102**(5), 050802 (2020)
19. N. Ohmae, M. Takamoto, Y. Takahashi, M. Kokubun, K. Araki, A. Hinton, I. Ushijima, T. Muramatsu, T. Furumiya, Y. Sakai, N. Moriya, N. Kamiya, K. Fujii, R. Muramatsu, T. Shiimado, H. Katori, Transportable Strontium optical lattice clocks operated outside laboratory at the level of 10^{-18} uncertainty. Adv. Quantum Tech. **4**(8), 2100015 (2021)
20. S. Origlia, M.S. Pramod, S. Schiller, Y. Singh, K. Bongs, R. Schwarz, A. Al-Masoudi, S. Dörscher, S. Herbers, S. Häfner, U. Sterr, C. Lisdat, Towards an optical clock for space: compact, high-performance optical lattice clock based on Bosonic atoms. Phys. Rev. A **98**(5), 053443 (2018)
21. The Laser Interferometer Space Antenna (LISA). https://www.elisascience.org
22. J. Luo, L.-S. Chen, H.-Z. Duan, Y.-G. Gong, S. Hu, J. Ji, Q. Liu, J. Mei, V. Milyukov, M. Sazhin, C.-G. Shao, V. T. Toth, H.-B. Tu, Y. Wang, Y. Wang, H.-C. Yeh, M.-S. Zhan, Y. Zhang, V. Zharov, Z.-B. Zhou. TianQin: A space-borne gravitational wave detector. arXiv:1512.02076 [astro-ph, physics:gr-qc] (2015)
23. W.-H. Ruan, Z.-K. Guo, R.-G. Cai, Y.-Z. Zhang. Taiji Program: Gravitational-Wave Sources. arXiv:1807.09495 [gr-qc, physics:hep-ph, physics:hep-th] (2018)
24. B. Argence, E. Prevost, T. Lévèque, R. Le Goff, S. Bize, P. Lemonde, G. Santarelli, Prototype of an ultra-stable optical cavity for space applications. Opt. Express **20**(23), 25409–25420 (2012)
25. S. Webster, P. Gill, Force-insensitive optical cavity. Opt. Lett. **36**(18), 3572–3574 (2011)
26. D.R. Leibrandt, M.J. Thorpe, M. Notcutt, R.E. Drullinger, T. Rosenband, J.C. Bergquist, Spherical reference cavities for frequency stabilization of lasers in non-laboratory environments. Opt. Express **19**(4), 3471–3482 (2011)
27. Q.-F. Chen, A. Nevsky, M. Cardace, S. Schiller, T. Legero, S. Häfner, A. Uhde, U. Sterr, A compact, robust, and transportable ultra-stable laser with a fractional frequency instability of 1×10^{-15}. Rev. Sci. Instrum. **85**(11), 113107 (2014)
28. S. Häfner, S. Herbers, S. Vogt, C. Lisdat, U. Sterr, Transportable interrogation laser system with an instability of Mod $\sigma_y = 3 \times 10^{-16}$. Opt. Express **28**(11), 16407–16416 (2020)
29. T. Legero, T. Kessler, U. Sterr, Tuning the thermal expansion properties of optical reference cavities with fused silica mirrors. J. Opt. Soc. Am. B **27**(5), 914–919 (2010)
30. B.-K. Tao, Q.-F. Chen, A vibration-insensitive-cavity design holds impact of higher than $100g$. Appl. Phys. B **124**(12), 228 (2018)
31. R.W.P. Drever, J.L. Hall, F.V. Kowalski, J. Hough, G.M. Ford, A.J. Munley, H. Ward, Laser phase and frequency stabilization using an optical resonator. Appl. Phys. B **31**(2), 97–105 (1983)
32. Z. Tai, L. Yan, Y. Zhang, X. Zhang, W. Guo, S. Zhang, H. Jiang, Electro-optic modulator with ultra-low residual amplitude modulation for frequency modulation and laser stabilization. Opt. Lett. **41**(23), 5584 (2016)
33. A. Didier, S. Ignatovich, E. Benkler, M. Okhapkin, T.E. Mehlstäubler, 946-nm Nd:YAG digital-locked laser at 1.1×10^{-16} in 1 s and transfer-locked to a cryogenic silicon cavity. Opt. Lett. **44**(7), 1781–1784 (2019)
34. P. Fang, H. Sun, Y. Wang, Y. Xu, Q. Chen, A self-reference direct-measuring scheme for precision optical frequency ratio measurement. Appl. Phys. B **128**(4), 73 (2022)
35. P. Fang, H. Sun, Y. Wang, Y. Xu, Q. Chen, Transfer of laser frequency from 729 nm to 1.5 μm with precision at the level of 10^{-20}. Chin. Opt. Lett. **20**(8), 5 (2022)